1-4-2013

Analysis of Small Molecule Ligands Targeting the HIV-1 Matrix Protein-RNA Binding Site

Ayna Alfadhli
Vollum Institute and Department of Microbiology, Oregon Health and Science University

Henry McNett
Vollum Institute and Department of Microbiology, Oregon Health and Science University

Jacob Eccles

Seyram Tsagli

Colleen Noviello

See next page for additional authors

Citation Details

Alfadhli, Ayna, Henry McNett, Jacob Eccles, Seyram Tsagli, Colleen Noviello, Rachel Sloan, Claudia S. López, David H. Peyton, and Eric Barklis. "Analysis of Small Molecule Ligands Targeting the HIV-1 Matrix Protein-RNA Binding Site." Journal of Biological Chemistry 288, no. 1 (2013): 666-676.

JBC Papers in Press. Published on November 7, 2012 as Manuscript M112.399865
The latest version is at http://www.jbc.org/cgi/doi/10.1074/jbc.M112.399865

ANALYSIS OF SMALL MOLECULE LIGANDS TARGETING THE HIV-1 MATRIX PROTEIN-RNA BINDING SITE

Ayna Alfadhli[1,3], Henry McNett[1], Jacob Eccles[1], Seyram Tsagli[1], Colleen Noviello[1], Rachel Sloan[1], Claudia S. López[1] , David H. Peyton[2] and Eric Barklis[1,3]

[1]Vollum Institute and Department of Microbiology, Oregon Health and Science University, 3181 SW Sam Jackson Park Road, Portland, Oregon 97201-3098
[2] Department of Chemistry, Portland State University, PO Box 751, Portland, Oregon 97207-0751

Running title: *Small molecule ligands of HIV-1 MA*

[3] Corresponding authors: TEL: 503-494-8098; FAX: 503-494-6862; emails: alfadhli@ohsu.edu, barklis@ohsu.edu

Keywords: HIV-1; Nuclear magnetic resonance; retrovirus; RNA; viral protein

Background: The HIV-1 matrix protein (MA) binds both RNA and phospholipids.
Results: Ligands that compete with RNA for binding to MA were identified and characterized.
Conclusion: Thiadiazolanes bind to residues in the HIV-1 MA β-II-V cleft that mediates RNA and phospholipid binding to MA.
Significance: These investigations provide new insights as to MA-ligand binding and antiviral design.

SUMMARY

The matrix (MA) domain of the HIV-1 PrGag protein directs PrGag proteins to assembly sites at the plasma membrane by virtue of its affinity to the phospholipid, phosphatidylinositol-4,5-bisphosphate ($PI(4,5)P_2$). MA also binds to RNA at a site that overlaps its $PI(4,5)P_2$ site, suggesting that RNA binding may protect MA from associating with inappropriate cellular membranes prior to PrGag delivery to the PM. Based on this, we have developed an assay in which small molecule competitors to MA-RNA binding can be characterized, with the assumption that such compounds might interfere with essential MA functions and help elucidate additional features of MA binding. Following this approach, we have identified four compounds, including three thiadiazolanes, that compete with RNA for MA binding. We also have identified MA residues involved in thiadiazolane binding and found that they overlap the MA $PI(4,5)P_2$ and RNA sites. Cell culture studies demonstrated that thiadiazolanes inhibit HIV-1 replication, but are associated with significant levels of toxicity. Nevertheless, these observations provide new insights as to MA binding, and pave the way for the development of antivirals that target the HIV-1 matrix domain.

INTRODUCTION

While current anti-HIV therapies target products of the *pol* gene, the development of drugs that target the HIV-1 Gag proteins, which direct virus assembly is of biomedical interest[1-6]. The HIV-1 matrix domain (MA) is the N-terminal cleavage product of the HIV-1 precursor Gag (PrGag) protein.

Initially, PrGag is synthesized on cytosolic ribosomes and becomes cotranslationally modified by the N-terminal attachment of a myristoyl group by N-myristoyl-transferase [7-9]. Myristoylated Gag precursors associate with the inner layer of the plasma membrane (PM), where they oligomerize, assemble, and bud off from cells as immature virions. During the maturation process, cleavage of PrGag by the viral protease (PR) generates the mature MA protein as well as capsid (CA), nucleocapsid (NC), p6 and two spacer peptides [5, 6]. The MA domain plays multiple roles in the viral replication cycle. One essential role of MA is the incorporation of the viral surface/transmembrane (SU/TM) envelope (Env) protein complex into virions [10-16]. Another essential function is to target PrGag proteins to their lipid raft-associated phosphatidylinositol-(4,5)-bisphosphate (PI[4,5]P_2) assembly sites at the PMs of infected cells [17-25]. Furthermore, MA oligomerization at membrane lipid rafts appears to trigger a myristate switch, in which the buried myristate group becomes exposed, and inserts into lipid bilayers, therefore promoting membrane binding [18, 23, 26-28]. In addition to membrane and Env protein binding, several reports have ascribed nucleic acid binding properties to retroviral MAs [29-35], and it is possible that such binding might facilitate PrGag delivery to the PM, virus assembly, and/ or nuclear import of viral preintegration complexes (PICs) [36-42].

How does the structure [27, 28, 32, 43-45] of MA accommodate all these essential functions? In addition to its N terminal myristate, which is essential for membrane binding [8, 25, 46, 47], MA is composed of globular domain consisting of 5 helices and three β sheet strands [27, 28, 43-45]. The membrane-binding face of HIV-1 MA is composed of a basic patch, promoting interactions with negatively charged phospholipid headgroups at the inner leaflets of PMs [27, 28, 43-45], and this patch selectively binds PI(4,5)P_2 [32-34, 45, 48, 49]. It has been shown that depletion of PM PI(4,5)P_2 by overexpression of polyphosphoinositide 5-phosphatase IV reduced HIV-1 assembly efficiency, resulting in the delivery of viral proteins to intracellular compartments [49, 50]. NMR investigations have indicated that HIV-1 MA preferentially binds to soluble PI(4,5)P_2 mimics through contacts with the lipid headgroup and its 2' acyl chain, and that binding promotes both exposure of the MA myristate group and protein oligomerization [28, 45]. Consistent with the above observations, we have shown that MA proteins tend to organize as hexamers of trimers on lipid membranes containing PI(4,5)P_2 [51], and that the binding specificity of MA is enhanced by cholesterol [32-33].

In addition to the MA membrane-binding to acidic lipids, several lines of experimentation have shown that HIV MA has a nucleic acid binding capacity that includes the highly basic region of MA [29-32, 34, 41, 42, 52-54]. Moreover, we have shown that RNA binding enhances the binding specificity of MA to PI(4,5)P_2-containing membranes. This was evident by the fact that PI(4,5)P_2-containing liposomes successfully competed with nucleic acids for MA binding, whereas other liposomes did not [32, 33]. In agreement with our results, RNAse treatment of Gag synthesized *in vitro* using rabbit reticulocyte lysate significantly reduced the selectivity of Gag binding to PI(4,5)P_2 liposomes as opposed to PS-containing liposomes [34]. We recently analyzed HIV MA interactions with RNA ligands that previously were selected for their high affinities to MA [30], and we identified MA residues that are involved in RNA binding evident by NMR chemical shift data [33]: interestingly, the RNA and PI(4,5)P_2 binding sites overlap. These and results from other labs [34, 55] suggest that RNA may provide a chaperone function in preventing Gag proteins from binding to membranes until they reach PI(4,5)P_2-rich plasma membranes.

To further characterize the binding properties of HIV-1 MA, we have identified and analyzed inhibitors of MA-RNA interactions. Specifically, using a competition assay for RNA binding to MA, we have identified a group of compounds that inhibit the MA-RNA binding activity. Interestingly, several such compounds are thiadiazolanes. We characterized these ligands with respect to their MA binding via nuclear magnetic

resonance spectroscopy (NMR), fluorescence anisotropy (FA), bead binding assays, and electrophoretic mobility shift assays (EMSA). Our studies demonstrate that MA-thiadiazolane binding sites overlap the MA-RNA and MA-PI(4,5)P_2 binding sites and identify residues in the β-II-V cleft and the C-terminus of helix II as binding elements. Moreover, thiadiazolanes were shown to inhibit HIV-1 replication in cell culture, but also demonstrated cytotoxicity. Despite this, our efforts provide new insights as to the nature of MA-RNA and MA-PI(4,5)P_2 binding sites, and open the door to the development of new classes of HIV antivirals.

EXPERIMENTAL PROCEDURES

Protein preparation. The myristoylated HIV-1 MA protein (MyrMA), as well as the unmyristoylated MA protein (MA), were expressed in *Escherichia coli* strain BL21(DE3)/pLysS (Novagen) along with *Saccharomyces cerevisiae N*-myristyltransferase from pET-11a-based vectors kindly provided by Michael F. Summers (University of Maryland Baltimore County) as described previously [27, 28, 32, 33, 45, 63]. The MA protein was prepared similarly to MyrMA, except that myristic acid was excluded from the bacterial growth media during the induction phase. The proteins were desalted by three rounds of buffer exchange using dialysis buffer of 10 mM sodium phosphate (pH 7.8) and 50 mM NaCl, supplemented with β-mercaptoethanol (BME; 1 mM final concentration), aliquoted, and stored at -80°C under nitrogen gas. ^{15}N isotopically labeled proteins were prepared by growing cells on $^{15}NH_4Cl$ (Cambridge Isotopes; NLM-467-5) as the sole nitrogen source as described previously [27, 28, 33, 43, 45, 63]. For NMR studies, the proteins were dialyzed against 50 mM sodium phosphate (pH 5.5), 100 mM NaCl and 5 mM dithiothreitol (DTT), and then concentrated by Millipore ultrafiltration concentrators against the same buffer. Protein purities were evaluated after fractionation by sodium dodecyl sulfate-polyacrylamide gel electrophoresis (SDS-PAGE; [32, 33, 64-68] by Coomassie blue staining [32, 64-66]. The HIV nucleocapsid (NC) peptide was prepared commercially as reported previously [68].

RNA Samples. The RNA oligomers used for our studies were selected for high affinity binding to MA [30, 33]. The consensus sequence for the high affinity RNA ligand to HIV-1 MA derived from screening of random 76 mer and 31 mer libraries as described previously [30, 31], yielding a consensus, 5'GGAAU UAAUA GUAGC3' (Sel15). We also prepared a 25mer stem-loop (Sel25) version of Sel15 that retained its high MA binding affinity: its sequence is 5' GGACA GGAAU UAAUA GUAGC UGUCC3'. As controls, we prepared a randomized version (Ran25) of Sel25, with the sequence of 5'GGACA GAAGG AGAUU UAUAC UGUCC3' and a randomized version of Sel15 with the sequence 5'GAAGG AGAUU UAUAC3'. In addition to the untagged RNAs, for plate binding studies, we procured biotinylated Sel15 and Sel25 RNAs from Invitrogen. We also procured fluorescently 5' tagged versions of Sel15, Ran15, Sel25, and Ran25 from Invitrogen. Another fluorescently labeled RNA corresponded to HIV-1 Mal isolate viral RNA (vRNA) nucleotides (nt) 1-4001. This was prepared by T7 RNA polymerase transcription from a SalI-linearized SP64HIV1-4005 plasmid (kindly provided by J.-C. Paillart, CNRS-Université de Strasbourg) as described previously[32] but with the use of 0.5 mM unlabeled nucleoside triphosphates plus 0.1 mM Cy3-CTP (GE Healthcare) in the transcription buffers.

Plate binding studies. Assay plates were 96 well nickel-NTA coated plates, purchased from Pierce and stored at 4 C°. Plate wells were coated with 2 μg of C-terminally his-tagged MyrMA in 100 ml sodium phosphate buffer (25mM NaPhos pH 7.8, 10mM NaCl) by 16 h 4°C binding incubations. Following this step, unbound proteins were removed from wells and wells were washed twice with 200 μl of incubation buffer (0.1 mg/ml bovine serum albumin [BSA], 25mM NaPhos pH 7.8, 10mM NaCl) using a plate washer (Multiwash III; Tricontinent). After

these washing steps, 250 nM biotinylated-Sel15 RNA was added in the presence of appropriate RNA-binding inhibition controls (dimethyl sulfoxide [DMSO], unlabeled RNA) or with compounds [in DMSO] to be tested in a final volume of 100 μl. Our compound library (Maybridge Hitfinder ;14,000 compounds) was available in 96-well plates and each compound was dissolved in DMSO to a concentration of 1 mM, with stock plates stored at -20°C. All controls (including 1 μl DMSO, 1.2 μM unlabeled Sel25 and Ran25, and no-protein mocks) were tested in every plate. The remaining columns were treated with 10 μM final concentrations of library compounds (1 μl of 1 mM). After 30 min incubations, unbound solutions were removed and plates were washed twice with 200 μl of incubation buffer per well. After the binding and washing steps, 4 μg/ml alkaline phosphatase-conjugated streptavidin (Invitrogen) in Dulbecco's Modified Eagles Media (DMEM) plus 10% calf sera was added and incubated for 45 min at 4° C. This was followed by removal of alkaline phosphatase and 5 washes of each well with 200 μl incubation buffer. The bound biotinylated-Sel15 RNA levels were detected by alkaline phosphatase reactions with 3 mg/ml substrate p-nitrophenyl phosphate (pNPhP; Sigma) in 1X assay salt (95 mM diethanolamine pH 9.85, 280 mM NaCl, 0.5 mM MgCl2). Absorbance was monitored at 420 nm (Molecular Device plate reader) for 10-60 min, and experimental samples were compared with controls from plates in which average positive control absorbance readings were 1.0. The effective inhibition by a given molecule from the library was calculated with respect to positive controls and absorbances normalized relative to DMSO controls were graphed. The hit threshold was set at ≤ 0.6 and qualifying compounds were retested in the secondary screen. Note that negative control values of samples supplemented with 1.2 μM Sel15 competitor were ten-fold lower than positive controls; that the Z screening window coefficient for positive and negative controls was 0.69; and that 1 mM guanidinium chloride, 1 mM EDTA, and 1% DMSO did not interfere with MA-RNA binding.

Fluorescence Polarization. Fluorescence polarization (fluorescence anisotropy [FA]) assays were used to measure inhibitor interference with MA-RNA binding. Measurements were conducted as described previously [33]. Measurements were obtained using a Pan Vera Beacon 2000 fluorescence polarizer (Invitrogen) with a 490 nm excitation wavelength. All readings were obtained at room temperature. For competition binding assays, samples of one ml of 5 nM FITC-labeled Sel15 RNA in pH 7.8 buffer (25 mM sodium phosphate [pH 7.8], 50 mM NaCl) plus or minus 1 μM MyrMA, were in 12 x 75 mm disposable borosilicate glass tubes. For competition, increasing concentrations of compounds or DMSO (as a control) were titrated from 0 to 60 μM. Polarization values correspond to emitted light intensities as defined by the ratio (parallel – perpendicular)/ (parallel + perpendicular); [69]). Competition assays were fitted assuming exponential decay binding curves using Prism (www.graphpad.com).

Competition electrophoretic mobility shift assays. RNA and MA samples were prepared in stocks containing 25 mM sodium phosphate (pH 7.8), 50 mM NaCl. For 20 μl binding reactions, 15 μM RNA was mixed with 15 μM MA in the presence of either 1 μl DMSO or 1 μl of 1 mM stock compounds in DMSO (50 μM final concentration). Samples were incubated at 35 °C for 30 min. Following incubations, samples were supplemented with 6 μl of 50% glycerol, and then loaded onto 12% native polyacrylamide (37.5:1 acrylamide: bis; polymerized with 0.0375% ammonium persulfate and 0.1125% TEMED) gels in 0.5 x Tris-borate buffer (44.5 mM Tris base, 44.5 mM boric acid, pH 8.0) [33, 70]. Gels were electrophoresed at 4 °C at 30–35 mA. For visualization of bound and free RNAs, gels were stained with Stains-all (Sigma),

destained by light exposure, and scanned immediately on an Epson Perfection 1240U scanner. Band intensities were obtained with Image J [32, 33, 66] software.

Bead binding assays. Bead binding assays followed our previously established protocols[32-33]. For the assays, 0.2 ml aliquots of packed nickel-nitrilotriacetic acid (Qiagen) beads were washed with 0.5 ml of wash buffer (25 mM sodium phosphate [pH 7.8], 50 mM NaCl, 0.1 mg/ml bovine serum albumin [Sigma A4503]), suspended in 0.5 ml of wash buffer supplemented with 20 μl of 10-mg/ml bovine serum albumin, incubated for 5 min at 4°C, and washed three times with 0.3 ml wash buffer. After the washes, packed beads were supplemented with 0.2 ml wash buffer plus 2-3 μg of his-tagged MyrMA. Proteins and beads were incubated for 2 h at 4°C, after which beads were pelleted, washed twice with 0.3 ml wash buffer, and suspended in a total volume of 360 μl wash buffer on ice: the estimated bead-bound MA concentration used in each assay was 300 nM.

For RNA competition binding assays, two fluorescently tagged RNAs were used. One was FITC-Sel25 (Invitrogen) and the second RNA corresponded to viral HIV-1 Mal isolate RNA nucleotides (nt) 1 to 4001, prepared as described in the RNA Samples section above. To perform competition assays, MyrMA-coated beads in 60 μl wash buffer were supplemented first with either 1 μl DMSO or 1 μl of stock compounds in DMSO (50 μM final concentration). Samples were incubated for 1 hour at 4°C. Following incubations, samples were supplemented with either FITC-Sel25 RNA (0.5 μM; 13 μM total nucleotide concentration) or HIV-1 viral RNA (nt 1-4001; 23 μM total nucleotide concentration), and incubated for 1 h at 4°C, after which beads were pelleted (1 min; 13,700 x g), quickly washed twice with 300 μl wash buffer, and resuspended in 60 μl of wash buffer on ice.

Liposome competition assays employed liposomes prepared as described previously[32] from stock solutions in chloroform of cholesterol (Sigma), 1,2-dioleoyl-sn-glycerol-3-phosphocholine (PC; Avanti), 1,2-dioleoyl-sn-glycero-3-phosphoethanolamine-N-(7-nitro-2-1,3benzoxadiazol-4-yl) (NBD-DOPE; Avanti), and brain phosphatidylinositol-(4,5)-bisphosphate [PI(4,5)P2 (Avanti)]. Lipids were dried in glass vials with a stream of nitrogen gas, supplemented with liposome buffer (10 mM HEPES [pH 7.4], 50 mM NaCl, 0.002% sodium azide), and suspended by twenty 30 second rounds of sonication in a Branson 1210 bath sonicator, with incubations on ice between each sonication round. Final liposome lipid concentrations were 2 mg/ml, and liposomes were stored for up to 1 week under nitrogen at –20°C. By weight, brain PI(4,5)P2 liposomes were prepared at 10% (wt/wt) and contained 20% cholesterol, 69.8% PC, and 0.2% NBD-DOPE. For liposome competition assays, MyrMA-coated beads were prepared and preincubated with DMSO or compounds in DMSO as described above. Samples so prepared were supplemented with 4 μg of liposomes, and incubated for 16-18 h at 4°C, after which beads were pelleted (1 min; 13,700 x g), quickly washed twice with 300 μl wash buffer, and resuspended in 50 μl of wash buffer on ice.

For viewing of fluorescent RNA or liposome ligands on MyrMA beads, samples were mixed by pipetting up and down and 10 μl samples were applied to microscope slides and covered with 22 mm by 22 mm coverslips. Fluorescent green beads were imaged on a Zeiss AxioPlan fluorescence microscope using a 20x (LDA-Plan) objective and Zeiss filter set 10 (excitation band-pass, 450 to 490; beam splitter Fourier transform, 510; emission band-pass, 515 to 565). For every individual experiment, exposure and gain settings were identical, and care was taken to make sure that brightness values (on a scale of 0 to 4,095) were below the maximum. After collection

of multiple bead images per sample as gray-scale tagged-image-file-format (TIFF) files using Improvision OpenLab software, images were ported to NIH Image J for analysis, as described previously[32–33]. For each bead, normalized bead brightness values were determined. To do so, areas and average brightness values were collected from circled beads. Average background brightness values were calculated by dividing total image average brightness values (with bead area brightness values zeroed out) by total image areas minus bead areas. Normalized bead brightness values (average bead brightness minus background brightness) were averaged for all beads of a given incubation in an experiment, and results of experiments were normalized to results with DMSO containing samples.

Tissue culture toxicity and efficacy assays. To test the compound toxicities, cells were treated with increasing compound concentrations and assayed for dehydrogenase levels using MTS (3-(4,5-dimethylthiazol-2-yl)-5-(3-carboxymethoxyphenyl)-2-(4-sulfophenyl)-2H-tetrazolium) substrate [62]. The assay measures the formation of a soluble formazan product that is proportional to the number of live cells in culture. Briefly, 293M cells (adherence adapted HEK 293T cells; [71, 72]) were plated at 15,000 cells per 96-well plate well in DMEM plus 10% fetal bovine serum (FBS) and incubated for 24 hours at 37°C/ 5% CO2. The supernatants were then removed, and cells were refed with 150 μl of DMEM plus 2% FBS, along with 1.5 μl DMSO or test compounds in 1.5 ml. The plates were incubated for 48 h, after which 30 μl of MTS reagent was added to each well. Plates then were incubated 60–90 min and read on a 96-well plate reader at 490 nm.

To test the effects on infectivity, a TZM-bl assay was employed. This assay employed CCR5+, CD4+ TZM-bl cells that express a β-galactosidase (β-gal) reporter when infected by HIV-1 [60, 61]. Briefly, human CEM-SS T cells cultured in RPMI plus 10% FBS were infected with HIV wild-type (wt) NL4-3 virus and left to incubate for 4 days. On the fourth day, infected CEM-SS cells were pelleted, washed three times with 10 ml RPMI, and re-suspended in 5 mL RPMI. Cells were counted and plated at 10,000 cells and 100 ml per well in RPMI plus 10% FBS per well on 96-well plates, treated with 1 μl of DMSO or compound in DMSO and incubated for 48 h. After 48 h, wells were supplemented with 75,000 TZM-bl cells (in 100 μl RPMI + 10 % FBS), treated with another 1 μl of DMSO or compound in DMSO and incubated for another 48 h. Following this incubation, supernatants were removed from the wells, and the adherent TZM-bl cells were lysed with 40 μl phosphate buffer saline (PBS) containing 0.1% sodium dodecyl sulfate (SDS). Following 5 min, wells of lysates were supplemented with 200 μl of 1X PM-2 (2mM MgSO4, 0.1mM MnCl2, 33mM NaH2PO4, 66mM Na2HPO4), containing 40 mM ß-Mercaptoethanol (BME) and 0.89 mg/ml ortho-nitrophenyl-ß-galactoside (ONPG). After 10-30 min incubations, the plates were read for absorbance at 420 nm. Signals for both TZM-bl and MTS assays were plotted as normalized values of DMSO controls.

NMR Spectroscopy. NMR data were collected at 35 °C on a Bruker Avance III (600 MHz ^{1}H) spectrometer, processed with Bruker-Topspin 2.1 software (BRUKER, http://www.bruker-biospin.com), and analyzed with NMRVIEW [73]. All of the NMR samples were prepared in a buffer containing 50 mM sodium phosphate at pH 5.5, 100 mM NaCl and 5 mM DTT using ^{15}N uniformly labeled protein samples of 80 μM (10% ^{2}H2O). Amide [^{1}HN–^{15}N] backbone cross-peaks for MA were observed using standard two dimensional (2D) heteronuclear sequential quantum correlation 2D [^{1}H–^{15}N] HSQC with pulse program hsqceftf3gp as described previously[74]. The 2D HSQC spectra were recorded as 2048 t2 x 256 t1 data points with 90° pulses for ^{1}H and ^{15}N of 10 μs and

36 μs respectively. These spectra were processed by Fourier transformation after zero-filling to 2048 x 1024 real data points, followed by phase and baseline correction. The 2D HSQC spectrum was recorded first with MA only. Signal assignments and verification of MA were matched with the chemical shift assignments that have been deposited at the BioMagResBank [27, 43]. The association of compounds and MA was monitored by observing the changes in the amide ^{1}HN–^{15}N cross-peaks in the HSQC spectra of ^{15}N labeled MA upon titration from 50 mM compound stock in DMSO as described previously [75]. Residues that exhibited significant chemical-shift changes upon titration with compounds or DMSO only were analyzed for the extent of the combined ^{1}H and ^{15}N (ΔδHN) chemical-shift changes by calculating $\Delta\delta HN = ([\Delta\delta\ ^{1}H]^2 + [\Delta\delta\ ^{15}N]^2)^{-1/2}$ [27, 45]. Binding isotherms from ^{1}H–^{15}N NMR HSQC titration experiments were calculated using Prism software (www.graphpad.com). Surface representations of the MA structure (pdb ID: 1UPH) were generated with PYMOL (http://pymol.sourceforge.net).

RESULTS

Identification of inhibitors of HIV-1 MA-RNA binding

Studies have shown that HIV MA possesses a nucleic acid binding activity that involves the highly basic region of MA [29-32, 34, 54]. Recently, we reported that RNA binding to MA acts as a chaperone which protects MA from associating with inappropriate cellular membranes prior to PrGag delivery to plasma membrane (PM) assembly sites [33]. Previously, *in vitro* selection experiments identified a 25mer aptamer Sel25 (GGACA GGAAU UAAUA GUAGC UGUCC) that showed high affinity binding to HIV-1 MA [30, 33]. The central fifteen nucleotides of Sel25, designated Sel15, also showed high affinity binding to the protein. Recently, we have characterized binding interactions of Sel15 RNA to MA, demonstrating that the MA RNA and $PI(4,5)P_2$ binding sites overlap [33].

To extend our previous observations, we developed an *in vitro* MA-RNA binding assay to identify potential inhibitors of MA-RNA interactions. Our assay involved binding C-terminally his-tagged MyrMA to 96 well nickel-NTA plates, incubation of the plates with biotin-Sel15 in the presence or absence of potential competitors, and colorimetric determination of bound biotin-Sel15 (see Experimental Procedures). Using the MA-RNA binding assay, we screened a library of 14,000 compounds for inhibition of MyrMA-Sel15 RNA binding, looking for candidates that significantly reduced Sel15 RNA binding to MyrMA. The robustness of the assay was indicated by the consistent large difference between samples containing no inhibitor and those using untagged Sel15 RNA as an inhibitor control. Moreover, we obtained a Z screening window coefficient for the primary screen of 0.69[56]. Because Z coefficients measure assay reliability, and ordinarily can vary from negative values to an optimum value of 1.0[56], our assay conditions appeared well-suited to inhibitor identification.

From the primary screen, 127 compounds that gave relative binding values of 0.6 or less were rescreened. Of these, 11 compounds gave primary screen values of 0.25 or less. Upon rescreening, five compounds consistently rescreened as binding inhibitors and four of these had given primary screen values of ≤ 0.25. Due to the unavailability of one of these compounds, four compounds (TD1, TD2, TD3, and DDD; Figure 1, Table 1) were obtained for further analysis. Interestingly, three of the four compounds (TD1, TD2 and TD3) are thiadiazolanes, and two other thiadiazolanes (TD4, TD5) were assayed in our primary screen. However, at 10 μM concentrations, TD4 and TD5 showed only modest inhibition of MA-RNA binding levels (Table 1). We also tested two glitazones (Figure 1), pioglitazone and rosiglitazone, that have a similar ring structure to thiadiazolanes, and which have been used to treat diabetes [57, 58]. When these compounds were tested at 10 μM concentrations, they failed to inhibit MA-RNA binding (Table 1). In contrast, primary and secondary screen values for TD1-3 and DDD (Table 1) earmarked them as potential binding inhibitors.

Characterization of MA-RNA binding inhibitors

To examine the specificities of compounds on MA-RNA binding, we employed native electrophoretic mobility shift assays (EMSA), using a native polyacrylamide gel electrophoresis (PAGE) system. As illustrated in Figure 2, 15 μM Sel25 or Sel15 RNAs and HIV-1 MyrMA (MA) or NC proteins were subjected to EMSAs. Binding of MA to Sel15 or Sel25 RNA resulted in RNA shift bands in the control sample and in the presence of DMSO, indicative of the formation of RNA-protein complexes (top two panels). However, RNA-Sel15 complex formation was diminished in the presence of 50 μM DDD (middle panel), while the same concentrations of compounds TD1-3 abolished MA binding to either RNA ligand. In contrast, when NC protein was incubated with Sel15 RNA and treated with either DMSO or the indicated compounds shown in Figure 2, shift bands (bottom panel; Figure 2) were not affected by compound treatment. These results demonstrate that DDD and TD1-3 specifically targeted MA-RNA interactions, but not RNA-NC binding. In addition, EMSA results imply that DDD and TD1-3 did not inhibit MA-plate binding via targeting his-tag interactions with Ni-NTA coated plates in the original assay system. In agreement with the EMSA results, and to rule out compound effects on MA-plate binding, MA-coated plates were treated with compounds, washed and tested for reactivity to anti-MA antibodies. No reductions of MA signals were observed (data not shown), supporting the notion that these compounds exert their inhibitory effects on MA-RNA complex formation.

To confirm the above results, we performed fluorescence anisotropy (FA) competition binding assays, where RNA ligands were fluorescently tagged, and the assay readout was via FA (Figure 3). Briefly, fluorescently tagged Sel15 RNA was incubated in the presence or absence of purified MA, and challenged with increasing concentrations of compounds. As illustrated in panel A, in the absence of MA, increasing concentrations of DMSO or compounds in DMSO led to diminutions of FA signals, probably due to fluorescence quenching [59]. However, in the presence of MA (panel B), results were different. Relative to DMSO, DDD did not have a significant effect on FA signals. In contrast, TD1-3 reduced RNA-MA binding levels. These results parallel our EMSA results (Figure 2), and demonstrate that the thiadiazolanes TD1-3 compete with Sel15 RNA for MA binding.

As another approach to assess compound effects on MyrMA-Sel RNA binding, we employed bead binding assays, as we have previously[32]. To do so, MyrMA-bound beads were incubated with fluorescently tagged Sel25 RNA in the presence of DMSO, TD1-3, or DDD. After incubations, Sel25 RNA binding levels were quantified and normalized to levels obtained in DMSO control incubations. Results from these assays (Figure 4A) were consistent with both EMSA (Figure 2) and FA (Figure 3) analyses, in that TD1-3 clearly reduced MyrMA-Sel RNA binding signals, whereas DDD did not. Because the bead binding protocol is compatible with the analysis of MA binding to longer RNAs, we also performed experiments with a fluorescently tagged 4001 nt RNA representing the 5' part of the HIV-1 genomic viral RNA. Results (Figure 4B) showed that DDD failed to inhibit HIV RNA binding to MyrMA. The thiodiazolanes had less profound effects on HIV RNA binding than on Sel25 RNA binding, possibly due to the capacity of the 4001 nt RNA to bind to a larger number of MyrMA monomers than the Sel25 RNA. Nevertheless, TD1-3 clearly gave reductions of HIV RNA-MA binding, consistent with a competition for the MA-RNA binding site. The bead binding assay also allowed us to examine the potential influence of compounds on the MA-PI(4,5)P_2 binding site, which overlaps the RNA binding site[33]. For this, MyrMA beads were incubated with DMSO or compounds, and then challenged with fluorescently tagged PI(4,5)P_2-containing liposomes, as we have previously[32-33]. Figure 4C demonstrates that DDD, TD3, TD2, and TD1 yielded increasing degrees of liposome binding inhibition. These observations support a model in which TDs occude overlapping MA RNA and PI(4,5)P_2 binding pockets.

Identification of binding site residues

To identify thiadiazolane (TD) binding site residues, NMR chemical shift perturbation experiments were performed.

For this assay, we tested TD1 (Figure 1) along with a DMSO control. The interactions between MA and TD1 were monitored by tracking chemical shifts in 2D HSQC spectra during titrations with TD1. This approach allows the identification of MA residues involved in ligand binding [28, 33, 45], and takes advantage of the fact that the MA NMR structure and databases for ^{1}H, and ^{15}N assignments were available [27, 43] to provide a baseline for our comparisons. For solubility reasons, we performed NMR HSQC experiments on unmyristoylated MA as previously done [33]. Initially, 2D ^{1}H-^{15}N HSQC spectra were collected for uniformly labeled MA, and assignments were cross-checked with the available assignments of MA: most of the anticipated cross-peaks were accounted for and matched the reported positions for MA ([27, 28, 43, 45]; Table 2). As illustrated in Figure 5A, high quality 2D HSQC spectra were obtained for MA upon titration with TD1. While the majority of signals were not sensitive to TD1 addition, titration of TD1 led to significant changes in the amide ^{1}H and ^{15}N chemical shifts of a subset of residues (Figure 5A-E, Table 2). In particular, we observed significant shifts (≥ 0.10 ppm) for residues Ser-6, Trp-16, Leu-21, Lys-32, Val-35, Glu-40, Leu-41, Arg-43, Val-46, Asn-47, Ile-60, Glu-73, Leu-75, Ser-77, Leu-78 (Table 2). Examples of data for Ala-100, which was unaffected by TD-1 binding, and for affected residues Leu-21, Lys-32 and Ser-77 are shown in Figures 5B-I. Interestingly, several shifted residues locate to the matrix protein β-II-V cleft, and some (residues Ser-6, Trp-16, Leu-21, Lys-73, Leu-75 and Ser-77) were shown previously to contribute to both PI(4,5)P_2 and RNA binding site [33, 45]. Thus, as anticipated, the TD1 binding site overlaps the MA binding site for RNA and PI(4,5)P_2 (Figure 6). These observations are discussed in more detail below.

Effects of inhibitors on virus infectivity and cell toxicity

To test the effects of DDD and TD1-3 on HIV-1 replication, TZM-bl assays were employed [60, 61]. In this case, HIV-1 infected CEM-SS T cells were treated with increasing concentrations of compounds and incubated in the presence of TZM-bl indicator cells, which express *E. coli* β-galactosidase (β-gal) when infected with HIV-1 [60, 61]. Due to the protocol employed (see Experimental Procedures), compound inhibition of any virus replication step may be detected. As shown in Figure 7, DDD and TD1-3 concentrations of 1-5 μM were sufficient to yield a 50% reduction (EC_{50}) of HIV-1 replication in this system. Unfortunately, when tested for cellular cytotoxicity using an MTS assay ([62]; Materials and Methods), DDD gave a 50% cytotoxic concentration (CC_{50}) of about 5 μM, while TD1-3 CC_{50} values ranged from 10-20 μM (Figure 6). These results imply that the DDD and TD scaffolds may be too toxic for anti HIV-1 drug development, but overall, our results suggest that it should be possible to target the MA PI(4,5)P_2-RNA binding pocket as a novel antiviral approach.

DISCUSSION

The matrix domain of the HIV-1 PrGag protein directs PrGag proteins to assembly sites at the PM, and facilitates the incorporation of full length HIV-1 envelope proteins into virions [10-25]. MA also has been shown to bind nucleic acids [29-35]. Recent experiments demonstrated that the ability of MA to bind RNA increases the selectivity of MA for PI(4,5)P_2-rich membrane assembly sites [32-34,55] . Based on these observations, we and others have proposed a chaperone model in which MA-RNA binding protected PrGag proteins from association with inappropriate intracellular membranes prior to delivery to the PI(4,5)P_2-rich PM [32-34,55]. Consistent with this model, our recent results indicate that the MA RNA and PI(4,5)P_2 binding sites overlap [33].

Based on the above observations, we reasoned that it might be possible to identify compounds that bind and possibly inhibit HIV-1 MA by virtue of their abilities to

interfere with MA binding to RNA. To this end, we developed a competitor screen in which compounds that inhibit MA-RNA binding were identified. Using this assay, we identified five compounds that consistently inhibited binding, four of which were available in higher quantities. As shown in Figure 1, one of these, DDD, is a naphthalene derivative. The other three (TD1-3) share the same thiadiazolane backbone that is closely related to the glitazone scaffold present on several drugs that have been used to treat type 2 diabetes (Figure 1; [57, 58]). Since two glitazones, pioglitazone and rosiglitazone, were available (Figure 1), we tested their abilities to inhibit MA-RNA binding, but found them inactive (Table 1). At this point, we do not know whether this inactivity is due to the glitazone scaffold itself, or to the specific R groups on pioglitazone and rosiglitazone.

To assess the specificities of the four compounds chosen from primary and secondary screens, we performed additional assays. EMSA assays demonstrated that DDD mildly inhibited MA-RNA binding, while TD1-3 significantly inhibited binding (Figure 2). These results complemented our initial observations and confirmed that thiadiazolanes do not simply block binding in a non-specific fashion. FA competition binding results (Figure 3) provided an independent confirmation of plate binding and EMSA assays, and yielded TD1-3 K_i inhibition constants in the 5-10 μM range (Figure 3). Bead binding assays additionally showed that thiodiazolanes reduced MA binding to an HIV-1 RNA fragment and PI(4,5)P_2-containing liposomes (Figure 4). To determine which MA residues might be involved in thiadiazolane binding, NMR chemical shift perturbation experiments with TD1were conducted. These investigations revealed that residues in the C-terminal portion of helix II (Glu-40, Leu-41, Arg-43), and several residues in the MA β-II-V cleft (Trp-16, Leu-21, Val-46, Lys-73, Leu-75 and Ser-77) were affected by titrations with a TD-1 compound (Figures 5-6). Interestingly, these β-II-V cleft residues previously were shown to contribute to both PI(4,5)P_2 and RNA binding [33, 45]. These data suggest that TD compounds act as competitive inhibitors of MA-RNA and MA-PI(4,5)P_2 interactions. It will be of interest to determine the structure of thiadiazolane-bound MA, both to verify this mechanism of action, and to help in the design of higher affinity MA ligands.

Despite their promising *in vitro* activities, TD1-3 showed somewhat disappointing *in vivo* inhibitory activities. Although they demonstrated EC_{50} concentrations of 1-5 μM (Figure 7), their cytotoxicities were such that therapeutic windows were only 3-5. At this point, we do not know whether the observed TD1-3 cytotoxicities stem from the thiadiazolane structure or are specific to these three thiadiazolanes. Nevertheless, our results clearly demonstrate the possibility of targeting the MA-PI(4,5)P_2-RNA binding pocket as a novel antiviral approach.

ACKNOWLEDGEMENTS

We are grateful to Michael F. Summers for bacterial expression vectors. We also appreciate the help and support of Robin Barklis and Mike Webb. This research was supported by National Institutes of Health grants GM060170, GM101983 and AI071798 to E.B.

REFERENCES

1. Larder, B. A. & Kemp, S. D. (1989). Multiple mutations in HIV-1 reverse transcriptase confer high-level resistance to zidovudine (AZT). *Science* **246**, 1155-1158.
2. Richman, D., Shih, C. K., Lowy, I., Rose, J., Prodanovich, P., Goff, S. & Griffin, J. (1991). Human immunodeficiency virus type 1 mutants resistant to nonnucleoside inhibitors of reverse transcriptase arise in tissue culture. *Proc Natl Acad Sci U S A* **88**, 11241-11245.
3. Moreno, S., Lopez Aldeguer, J., Arribas, J. R., Domingo, P., Iribarren, J. A., Ribera, E., Rivero, A. & Pulido, F. (2010). The future of antiretroviral therapy: challenges and needs. *J Antimicrob Chemother* **65**, 827-835.

4. Coffin, J. M., Hughes, S. H. & Varmus, H. E. (1997). The Interactions of Retroviruses and their Hosts. In J. Coffin, S. Hughes, and H. Varmus (ed.), *Retroviruses*. Cold Spring Harbor Laboratory Press, Cold Spring Harbor, NY.
5. Freed, E. O. (1998). HIV-1 gag proteins: diverse functions in the virus life cycle. *Virology* **251**, 1-15.
6. Swanstrom, R. & Wills, J. W. (1997). Synthesis, Assembly, and Processing of Viral Proteins. In J. Coffin, S. Hughes, and H. Varmus (ed.), *Retroviruses*. Cold Spring Harbor Laboratory Press, Cold Spring Harbor, NY. 263-334.
7. Mervis, R. J., Ahmad, N., Lillehoj, E. P., Raum, M. G., Salazar, F. H., Chan, H. W. & Venkatesan, S. (1988). The gag gene products of human immunodeficiency virus type 1: alignment within the gag open reading frame, identification of posttranslational modifications, and evidence for alternative gag precursors. *J Virol* **62**, 3993-4002.
8. Bryant, M. & Ratner, L. (1990). Myristoylation-dependent replication and assembly of human immunodeficiency virus 1. *Proc Natl Acad Sci U S A* **87**, 523-527.
9. Tritel, M. & Resh, M. D. (2000). Kinetic analysis of human immunodeficiency virus type 1 assembly reveals the presence of sequential intermediates. *J Virol* **74**, 5845-5855.
10. Yu, X., Yuan, X., Matsuda, Z., Lee, T. H. & Essex, M. (1992). The matrix protein of human immunodeficiency virus type 1 is required for incorporation of viral envelope protein into mature virions. *J Virol* **66**, 4966-4971.
11. Davis, M. R., Jiang, J., Zhou, J., Freed, E. O. & Aiken, C. (2006). A mutation in the human immunodeficiency virus type 1 Gag protein destabilizes the interaction of the envelope protein subunits gp120 and gp41. *J Virol* **80**, 2405-2417.
12. Dorfman, T., Bukovsky, A., Ohagen, A., Hoglund, S. & Gottlinger, H. G. (1994). Functional domains of the capsid protein of human immunodeficiency virus type 1. *J Virol* **68**, 8180-8187.
13. Freed, E. O. & Martin, M. A. (1995). The role of human immunodeficiency virus type 1 envelope glycoproteins in virus infection. *J Biol Chem* **270**, 23883-23886.
14. Freed, E. O. & Martin, M. A. (1996). Domains of the human immunodeficiency virus type 1 matrix and gp41 cytoplasmic tail required for envelope incorporation into virions. *J Virol* **70**, 341-351.
15. Wyma, D. J., Kotov, A. & Aiken, C. (2000). Evidence for a stable interaction of gp41 with Pr55(Gag) in immature human immunodeficiency virus type 1 particles. *J Virol* **74**, 9381-9387.
16. Checkley, M. A., Luttge, B. G. & Freed, E. O. (2011). HIV-1 envelope glycoprotein biosynthesis, trafficking, and incorporation. *J Mol Biol* **410**, 582-608.
17. Bhatia, A. K., Campbell, N., Panganiban, A. & Ratner, L. (2007). Characterization of replication defects induced by mutations in the basic domain and C-terminus of HIV-1 matrix. *Virology* **369**, 47-54.
18. Bouamr, F., Scarlata, S. & Carter, C. (2003). Role of myristylation in HIV-1 Gag assembly. *Biochemistry* **42**, 6408-6417.
19. Dalton, A. K., Ako-Adjei, D., Murray, P. S., Murray, D. & Vogt, V. M. (2007). Electrostatic interactions drive membrane association of the human immunodeficiency virus type 1 Gag MA domain. *J Virol* **81**, 6434-6445.
20. Ehrlich, L. S., Fong, S., Scarlata, S., Zybarth, G. & Carter, C. (1996). Partitioning of HIV-1 Gag and Gag-related proteins to membranes. *Biochemistry* **35**, 3933-3943.
21. Jouvenet, N., Neil, S. J., Bess, C., Johnson, M. C., Virgen, C. A., Simon, S. M. & Bieniasz, P. D. (2006). Plasma membrane is the site of productive HIV-1 particle assembly. *PLoS Biol* **4**, e435.
22. Murray, P. S., Li, Z., Wang, J., Tang, C. L., Honig, B. & Murray, D. (2005). Retroviral matrix domains share electrostatic homology: models for membrane binding function throughout the viral life cycle. *Structure* **13**, 1521-1531.
23. Scarlata, S., Ehrlich, L. S. & Carter, C. A. (1998). Membrane-induced alterations in HIV-1 Gag and matrix protein-protein interactions. *J Mol Biol* **277**, 161-169.
24. Scholz, I., Still, A., Dhenub, T. C., Coday, K., Webb, M. & Barklis, E. (2008). Analysis of human immunodeficiency virus matrix domain replacements. *Virology* **371**, 322-335.

25. Spearman, P., Wang, J. J., Vander Heyden, N. & Ratner, L. (1994). Identification of human immunodeficiency virus type 1 Gag protein domains essential to membrane binding and particle assembly. *J Virol* **68**, 3232-3242.
26. Resh, M. D. (2004). A myristoyl switch regulates membrane binding of HIV-1 Gag. *Proc Natl Acad Sci U S A* **101**, 417-418.
27. Tang, C., Loeliger, E., Luncsford, P., Kinde, I., Beckett, D. & Summers, M. F. (2004). Entropic switch regulates myristate exposure in the HIV-1 matrix protein. *Proc Natl Acad Sci U S A* **101**, 517-522.
28. Saad, J. S., Loeliger, E., Luncsford, P., Liriano, M., Tai, J., Kim, A., Miller, J., Joshi, A., Freed, E. O. & Summers, M. F. (2007). Point mutations in the HIV-1 matrix protein turn off the myristyl switch. *J Mol Biol* **366**, 574-585.
29. Ott, D. E., Coren, L. V. & Gagliardi, T. D. (2005). Redundant roles for nucleocapsid and matrix RNA-binding sequences in human immunodeficiency virus type 1 assembly. *J Virol* **79**, 13839-13847.
30. Purohit, P., Dupont, S., Stevenson, M. & Green, M. R. (2001). Sequence-specific interaction between HIV-1 matrix protein and viral genomic RNA revealed by in vitro genetic selection. *RNA* **7**, 576-584.
31. Lochrie, M. A., Waugh, S., Pratt, D. G. J., Clever, J., Parslow, T. G. & Polisky, B. (1997). In vitro selection of RNAs that bind to the human immunodeficiency virus type-1 gag polyprotein. *Nucleic Acids Res* **25**, 2902-2910.
32. Alfadhli, A., Still, A. & Barklis, E. (2009). Analysis of human immunodeficiency virus type 1 matrix binding to membranes and nucleic acids. *J Virol* **83**, 12196-12203.
33. Alfadhli, A., McNett, H., Tsagli, S., Bachinger, H. P., Peyton, D. H. & Barklis, E. (2011). HIV-1 Matrix Protein Binding to RNA. *J Mol Biol* **410**, 653-666.
34. Chukkapalli, V., Oh, S. J. & Ono, A. (2010). Opposing mechanisms involving RNA and lipids regulate HIV-1 Gag membrane binding through the highly basic region of the matrix domain. *Proc Natl Acad Sci U S A* **107**, 1600-1605.
35. Monde, K., Chukkapalli, V. & Ono, A. (2011). Assembly and replication of HIV-1 in T cells with low levels of phosphatidylinositol-(4,5)-bisphosphate. *J Virol* **85**, 3584-3595.
36. Bukrinsky, M. I., Haggerty, S., Dempsey, M. P., Sharova, N., Adzhubel, A., Spitz, L., Lewis, P., Goldfarb, D., Emerman, M. & Stevenson, M. (1993). A nuclear localization signal within HIV-1 matrix protein that governs infection of non-dividing cells. *Nature* **365**, 666-669.
37. von Schwedler, U., Kornbluth, R. S. & Trono, D. (1994). The nuclear localization signal of the matrix protein of human immunodeficiency virus type 1 allows the establishment of infection in macrophages and quiescent T lymphocytes. *Proc Natl Acad Sci U S A* **91**, 6992-6996.
38. Miller, M. D., Farnet, C. M. & Bushman, F. D. (1997). Human immunodeficiency virus type 1 preintegration complexes: studies of organization and composition. *J Virol* **71**, 5382-5390.
39. Reil, H., Bukovsky, A. A., Gelderblom, H. R. & Gottlinger, H. G. (1998). Efficient HIV-1 replication can occur in the absence of the viral matrix protein. *EMBO J* **17**, 2699-2708.
40. Haffar, O. K., Popov, S., Dubrovsky, L., Agostini, I., Tang, H., Pushkarsky, T., Nadler, S. G. & Bukrinsky, M. (2000). Two nuclear localization signals in the HIV-1 matrix protein regulate nuclear import of the HIV-1 pre-integration complex. *J Mol Biol* **299**, 359-368.
41. Hearps, A. C., Wagstaff, K. M., Piller, S. C. & Jans, D. A. (2008). The N-terminal basic domain of the HIV-1 matrix protein does not contain a conventional nuclear localization sequence but is required for DNA binding and protein self-association. *Biochemistry* **47**, 2199-2210.
42. Cai, M., Huang, Y., Craigie, R. & Clore, G. M. (2010). Structural basis of the association of HIV-1 matrix protein with DNA. *PLoS One* **5**, e15675.
43. Massiah, M. A., Starich, M. R., Paschall, C., Summers, M. F., Christensen, A. M. & Sundquist, W. I. (1994). Three-dimensional structure of the human immunodeficiency virus type 1 matrix protein. *J Mol Biol* **244**, 198-223.

44. Hill, C. P., Worthylake, D., Bancroft, D. P., Christensen, A. M. & Sundquist, W. I. (1996). Crystal structures of the trimeric human immunodeficiency virus type 1 matrix protein: implications for membrane association and assembly. *Proc Natl Acad Sci U S A* **93**, 3099-3104.
45. Saad, J. S., Miller, J., Tai, J., Kim, A., Ghanam, R. H. & Summers, M. F. (2006). Structural basis for targeting HIV-1 Gag proteins to the plasma membrane for virus assembly. *Proc Natl Acad Sci U S A* **103**, 11364-11369.
46. Freed, E. O., Orenstein, J. M., Buckler-White, A. J. & Martin, M. A. (1994). Single amino acid changes in the human immunodeficiency virus type 1 matrix protein block virus particle production. *J Virol* **68**, 5311-5320.
47. Gottlinger, H. G., Sodroski, J. G. & Haseltine, W. A. (1989). Role of capsid precursor processing and myristoylation in morphogenesis and infectivity of human immunodeficiency virus type 1. *Proc Natl Acad Sci U S A* **86**, 5781-5785.
48. Shkriabai, N., Datta, S. A., Zhao, Z., Hess, S., Rein, A. & Kvaratskhelia, M. (2006). Interactions of HIV-1 Gag with assembly cofactors. *Biochemistry* **45**, 4077-4083.
49. Chukkapalli, V., Hogue, I. B., Boyko, V., Hu, W. S. & Ono, A. (2008). Interaction between the human immunodeficiency virus type 1 Gag matrix domain and phosphatidylinositol-(4,5)-bisphosphate is essential for efficient gag membrane binding. *J Virol* **82**, 2405-2417.
50. Ono, A., Ablan, S. D., Lockett, S. J., Nagashima, K. & Freed, E. O. (2004). Phosphatidylinositol (4,5) bisphosphate regulates HIV-1 Gag targeting to the plasma membrane. *Proc Natl Acad Sci U S A* **101**, 14889-14894.
51. Alfadhli, A., Barklis, R. L. & Barklis, E. (2009). HIV-1 matrix organizes as a hexamer of trimers on membranes containing phosphatidylinositol-(4,5)-bisphosphate. *Virology* **387**, 466-472.
52. Burniston, M. T., Cimarelli, A., Colgan, J., Curtis, S. P. & Luban, J. (1999). Human immunodeficiency virus type 1 Gag polyprotein multimerization requires the nucleocapsid domain and RNA and is promoted by the capsid-dimer interface and the basic region of matrix protein. *J Virol* **73**, 8527-8540.
53. Chang, C. Y., Chang, Y. F., Wang, S. M., Tseng, Y. T., Huang, K. J. & Wang, C. T. (2008). HIV-1 matrix protein repositioning in nucleocapsid region fails to confer virus-like particle assembly. *Virology* **378**, 97-104.
54. Jones, C. P., Datta, S. A., Rein, A., Rouzina, I. & Musier-Forsyth, K. (2011). Matrix domain modulates HIV-1 Gag's nucleic acid chaperone activity via inositol phosphate binding. *J Virol* **85**, 1594-1603.
55. Chukkapalli, V. & Ono, A. (2011). Molecular determinants that regulate plasma membrane association of HIV-1 Gag. *J Mol Biol* **410**, 512-524.
56. Zhang, J. H., Chung, T. D. & Oldenburg, K. R. (1999). A Simple Statistical Parameter for Use in Evaluation and Validation of High Throughput Screening Assays. *J Biomol Screen* **4**, 67-73.
57. Chen, Z., Vigueira, P. A., Chambers, K. T., Hall, A. M., Mitra, M. S., Qi, N., McDonald, W. G., Colca, J. R., Kletzien, R. F. & Finck, B. N. (2012). Insulin Resistance and Metabolic Derangements in Obese Mice are Ameliorated by a Novel Peroxisome Proliferator-Activated Receptor gamma-sparing Thiazolidinedione. *J Biol Chem*
58. Smith, U. (2001). Pioglitazone: mechanism of action. *Int J Clin Pract Suppl* 13-18.
59. Moldt, P., Andersen, W. K. & Christensen, S. B. (1988). Dimethyl sulfoxide decreases the fluorescence yield of the reaction between histamine and ortho-phthalaldehyde and may influence histamine release. *Agents Actions* **24**, 35-39.
60. Platt, E. J., Wehrly, K., Kuhmann, S. E., Chesebro, B. & Kabat, D. (1998). Effects of CCR5 and CD4 cell surface concentrations on infections by macrophagetropic isolates of human immunodeficiency virus type 1. *J Virol* **72**, 2855-2864.
61. Wei, X., Decker, J. M., Liu, H., Zhang, Z., Arani, R. B., Kilby, J. M., Saag, M. S., Wu, X., Shaw, G. M. & Kappes, J. C. (2002). Emergence of resistant human immunodeficiency virus type 1 in patients receiving fusion inhibitor (T-20) monotherapy. *Antimicrob Agents Chemother* **46**, 1896-1905.

62. Cory, A. H., Owen, T. C., Barltrop, J. A. & Cory, J. G. (1991). Use of an aqueous soluble tetrazolium/formazan assay for cell growth assays in culture. *Cancer Commun* **3**, 207-212.
63. Ghanam, R. H., Fernandez, T. F., Fledderman, E. L. & Saad, J. S. (2010). Binding of calmodulin to the HIV-1 matrix protein triggers myristate exposure. *J Biol Chem* **285**, 41911-41920.
64. Alfadhli, A., Dhenub, T. C., Still, A. & Barklis, E. (2005). Analysis of human immunodeficiency virus type 1 Gag dimerization-induced assembly. *J Virol* **79**, 14498-14506.
65. Alfadhli, A., Huseby, D., Kapit, E., Colman, D. & Barklis, E. (2007). Human immunodeficiency virus type 1 matrix protein assembles on membranes as a hexamer. *J Virol* **81**, 1472-1478.
66. Barklis, E., Alfadhli, A., McQuaw, C., Yalamuri, S., Still, A., Barklis, R. L., Kukull, B. & Lopez, C. S. (2009). Characterization of the in vitro HIV-1 capsid assembly pathway. *J Mol Biol* **387**, 376-389.
67. Wang, C. T., Zhang, Y., McDermott, J. & Barklis, E. (1993). Conditional infectivity of a human immunodeficiency virus matrix domain deletion mutant. *J Virol* **67**, 7067-7076.
68. Zuber, G., McDermott, J., Karanjia, S., Zhao, W., Schmid, M. F. & Barklis, E. (2000). Assembly of retrovirus capsid-nucleocapsid proteins in the presence of membranes or RNA. *J Virol* **74**, 7431-7441.
69. Lundblad, J. R., Laurance, M. & Goodman, R. H. (1996). Fluorescence polarization analysis of protein-DNA and protein-protein interactions. *Mol Endocrinol* **10**, 607-612.
70. Zhou, J., McAllen, J. K., Tailor, Y. & Summers, M. F. (2005). High affinity nucleocapsid protein binding to the muPsi RNA packaging signal of Rous sarcoma virus. *J Mol Biol* **349**, 976-988.
71. DuBridge, R. B., Tang, P., Hsia, H. C., Leong, P. M., Miller, J. H. & Calos, M. P. (1987). Analysis of mutation in human cells by using an Epstein-Barr virus shuttle system. *Mol Cell Biol* **7**, 379-387.
72. Noviello, C. M., Lopez, C. S., Kukull, B., McNett, H., Still, A., Eccles, J., Sloan, R. & Barklis, E. (2011). Second-Site Compensatory Mutations of HIV-1 Capsid Mutations. *J Virol* **85**, 4730-4738.
73. Johnson, B. A. & Blevins, R. A. (1994). NMR View: a computer program for the visualization and analysis of NMR data. *J Biomol NMR* **4**, 603-614.
74. Davis, A. L., Keeler, J., Laue, E. D. & Moskau, D. (1992). Experiments for recording pure-absorption heteronuclear correlation spectra using pulsed field gradients. *J Magn Reson* **98**, 207-216.
75. Tang, C., Loeliger, E., Kinde, I., Kyere, S., Mayo, K., Barklis, E., Sun, Y., Huang, M. & Summers, M. F. (2003). Antiviral inhibition of the HIV-1 capsid protein. *J Mol Biol* **327**, 1013-1020.

TABLE AND FIGURE LEGENDS

Table 1. Plate binding assay values for MyrMA-RNA binding inhibitors and analogues. Plate binding assays of MyrMA-Sel15 RNA binding inhibition were performed with 10 μM concentrations of inhibitor candidates as described in the Experimental Procedures section. Values listed correspond to MyrMA-RNA binding signals normalized to DMSO controls such that a value of 1.0 is equivalent to the DMSO control and indicates no inhibition, whereas lower values are indicative of binding inhibition. Available compounds with normalized primary screen values of $\leq$0.6 were rescreened in triplicate in secondary assays Due to unavailability or lack of inhibitory activity, secondary screening of the compounds TD4, TD5, pioglitazone, and rosiglitazone was not done (ND).

Table 2. MA residues showing significant chemical shifts on TD1 binding. ^{1}H-^{15}N NMR chemical shifts observed for MA bound to TD1 at pH 5.5 and 35°C are tabulated. The association of TD1 and MA was monitored by observing changes in the ^{1}H–^{15}N cross-peaks in the HSQC spectra of ^{15}N labeled MA upon titration with TD1. Shown are residues that exhibited significant chemical shifts ($\geq$ 0.10 ppm) upon titrations with TD1. The extent of the combined ^{1}H and ^{15}N (ΔδHN) chemical-shift changes was calculated according to the formula $\Delta\delta HN = ((\Delta\delta\ ^{1}H)^2 + (\Delta\delta\ ^{15}N)^2\ )^{-}$. Indicated are the final ΔδHN titrations of TD1 with TD1: MA ratio of 16:1.

Figure 1. Chemical structures of MyrMA-RNA binding inhibitors and analogues. The compounds TD1 (2-(2-chloro-6-methylphenyl)-4-(cyclopropylmethyl)-1,2,4-thiadiazolane-3,5-dione; 296.8 Da), TD2 (4-methyl-2-(1-naphthyl)-1,2,4-thiadiazolane-3,5-dione; 258.3 Da), TD3 (4-(cyclopropylmethyl)-2-(3,5-dimethylisoxazol-4-yl)-1,2,4-thiadiazolane-3,5-dione ; 267.3 Da), and DDD (2,3-dichloro-1,4-dihydronaphthalene-1,4-dione; 227 Da) were observed in screens to inhibit MyrMA-RNA binding. Also shown are the general structures of thiadiazolane-3,5-diones and related glitazones. Note that other thiadiazolane-3,5-diones screened were TD4 (2-(2-chloro-6-methylphenyl)-4-(cyclopropylmethyl)-1,2,4-thiadiazolane-3,5-dione) and TD5 (2-(3,5-dimethylisoxazol-4-yl)-4-(4-fluorophenyl)- 1,2,4-thiadiazolane-3,5-dione) ; and that the glitazones pioglitazone (5-((4(2-(5-ethylpyridin-2-yl)ethoxy)phenylmethyl)-1,3- thiadiazolane-2,4-dione) and rosiglitazone ((RS)-5-4-2-(methyl(pyridin-2-yl)amino)ethoxybenzyl) thiadiazolane-2,4-dione) also were assayed.

Figure 2. Electrophoretic mobility shift assays. Electrophoretic mobility shift assays (EMSA) were performed with 15 μM Sel25 or Sel15 RNAs and 15 μM concentrations of HIV-1 MyrMA (MA) or NC proteins as indicated. In each panel, the far right lane represents an RNA only incubation and the leftmost five lanes represent assays performed in the presence of 1 ml (5%) DMSO or 50 μM final concentrations of the indicated compounds in DMSO. Bound (B) and free (F) RNAs were detected after electrophoresis by staining. Note that TD1-3 impaired RNA binding to MyrMA but not to NC.

Figure 3. Fluorescence anisotropy competition binding assays. FA competition binding assays were performed with 5 nM FITC-Sel15 in the absence (panel A) or presence (panel B) of 1 μM MyrMA and increasing concentrations of compounds or DMSO (as a control) that were titrated to achieve final compound concentrations of 0-60 μM. Competition assays were plotted as millipolarization versus inhibitor concentration and fitted assuming exponential decay binding curves. Note that DMSO and all compounds in DMSO reduced FA signals of free FITC-Sel15, presumably due to probe quenching (panel A). However, in the presence of MyrMA (panel B), the compounds TD1-3 showed greater effects on FA signals than DMSO or DDD, consistent with reductions in MyrMA-RNA binding levels.

Figure 4. Fluorescent bead binding assays. MyrMA beads were incubated either with DMSO (control) or with 50 μM concentrations of the indicated compounds, and then supplemented with either 0.5 μM

FITC-Sel25 RNA **(A)**, fluorescently labeled HIV-1 viral RNA (nt 1-4001; 23 μM total nucleotide concentration) **(B)**, or 4 μg NBD-DOPE-tagged PI(4,5)P_2-containing liposomes **(C)**. Following binding incubations, beads were pelleted, washed, resuspended in wash buffer, and imaged by fluorescence microscopy under identical gain and exposure settings. For quantitation, background-subtracted bead brightness values were calculated, averaged from multiple ($n \geq 8$) beads for each incubation, and normalized to DMSO control samples. Fluorescent ligand binding values are plotted relative to DMSO controls in each panel.

Figure 5. NMR of MA-TD1 binding. (A) Shown is an overlay of 2D ^{1}H-^{15}N HSQC spectra of ^{15}N-labeled MA obtained at pH 5.5 and 35°C upon titration with TD1 at the following TD1: MA ratios: 0:1 (black), 1:1 (blue), 4:1(green), 8:1 (yellow), and 16:1 (red). Indicated in circles are some of the shifted residues. **B-E** show representative expanded portions of the 2D ^{1}H-^{15}N HSQC overlay, with the same titrations ratios as in **(A)**. **F-I** show binding curves of ^{1}H-^{15}N NMR chemical shift titration data from panels B-E. Note that residue A100 is provided as an example of a residue that is not affected by drug binding, whereas L21, K32, and S77 are examples of residues that were affected by binding.

Figure 6. MA binding sites of TD1, RNA and PI(4,5)P_2. Shown are surface representations of MA (pdb ID: 1UPH). Residues that exhibited significant chemical shift changes ($\Delta\delta HN \geq 0.10$ ppm) on TD1 binding are colored in blue (A); Sel15 RNA binding residues are highlighted in red (B); and di-C_4-PI(4,5)P_2 binding residues are highlighted in green (C). For convenience a subset of the binding residues is labeled.

Figure 7. Cell culture toxicity and virus replication assays. Cell culture toxicity (circles) and anti-HIV-1 inhibition assays (boxes) were performed as described in the Materials and Methods with various concentrations of the indicated compounds. Results are plotted as graphs of percentage of cell viability or virus replication relative to mock (DMSO) controls, versus compound concentrations.

Compound	1° screen	2° screen
DDD	0.58	0.48 +/- 0.17
TD1	0.09	0.19 +/- 0.03
TD2	0.08	0.12 +/- 0.06
TD3	0.11	0.34 +/- 0.09
TD4	0.47	ND
TD5	0.70	ND
pioglitazone	0.93	ND
rosiglitazone	0.95	ND

Table 1. Plate binding assay values for MyrMA-RNA binding inhibitors and analogues. Plate binding assays of MyrMA-Sel15 RNA binding inhibition were performed with 10 μM concentrations of inhibitor candidates as described in the Experimental Procedures section. Values listed correspond to MyrMA-RNA binding signals normalized to DMSO controls such that a value of 1.0 is equivalent to the DMSO control and indicates no inhibition, whereas lower values are indicative of binding inhibition. Available compounds with normalized primary screen values of $\leq$0.6 were rescreened in triplicate in secondary assays Due to unavailability or lack of inhibitory activity, secondary screening of the compounds TD4, TD5, pioglitazone, and rosiglitazone was not done (ND).

Residue	$\Delta\delta^{1}H$-^{15}N ($\geq$ 0.10 ppm)
6 Ser	0.11
16 Trp	0.17
21 Leu	0.11
32 Lys	0.12
35 Val	0.12
40 Glu	0.11
41 Leu	0.16
43 Arg	0.10
46 Val	0.10
47 Asn	0.15
60 Ile	0.11
73 Glu	0.16
75 Leu	0.21
77 Ser	0.12
78 Leu	0.10

Table 2. MA residues showing significant chemical shifts on TD1 binding. ^{11}H-^{15}N NMR chemical shifts observed for MA bound to TD1 at pH 5.5 and 35°C are tabulated. The association of TD1 and MA was monitored by observing changes in the ^{1}H–^{15}N cross-peaks in the HSQC spectra of ^{15}N labeled MA upon titration with TD1. Shown are residues that exhibited significant chemical shifts ($\geq$ 0.10 ppm) upon titrations with TD1. The extent of the combined ^{1}H and ^{15}N ($\Delta\delta HN$) chemical-shift changes was calculated according to the formula $\Delta\delta HN = ((\Delta\delta\ ^{1}H)^2 + (\Delta\delta\ ^{15}N)^2\ )^{-1/2}$. Indicated are the final $\Delta\delta HN$ titrations of TD1 with TD1: MA ratio of 16:1.

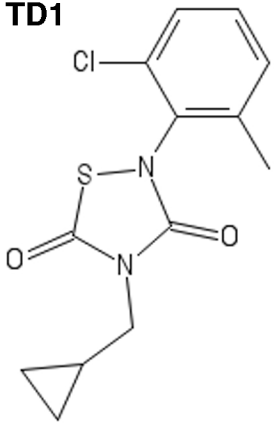

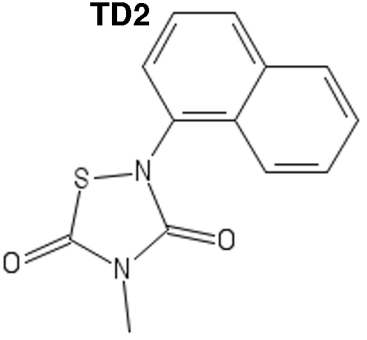

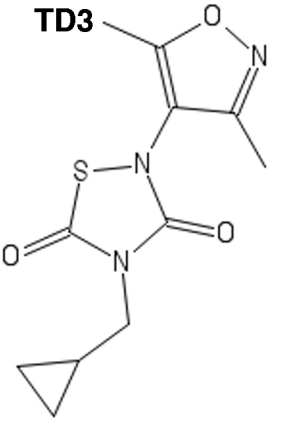

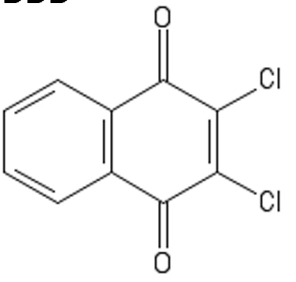

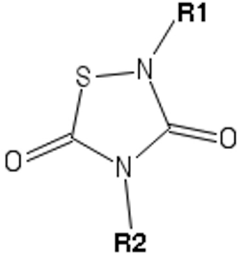

other thiodiazolanes:
TD4
TD5

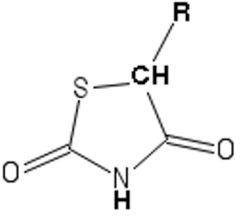

glitazones:
pioglitazone
rosiglitazone

Figure 1

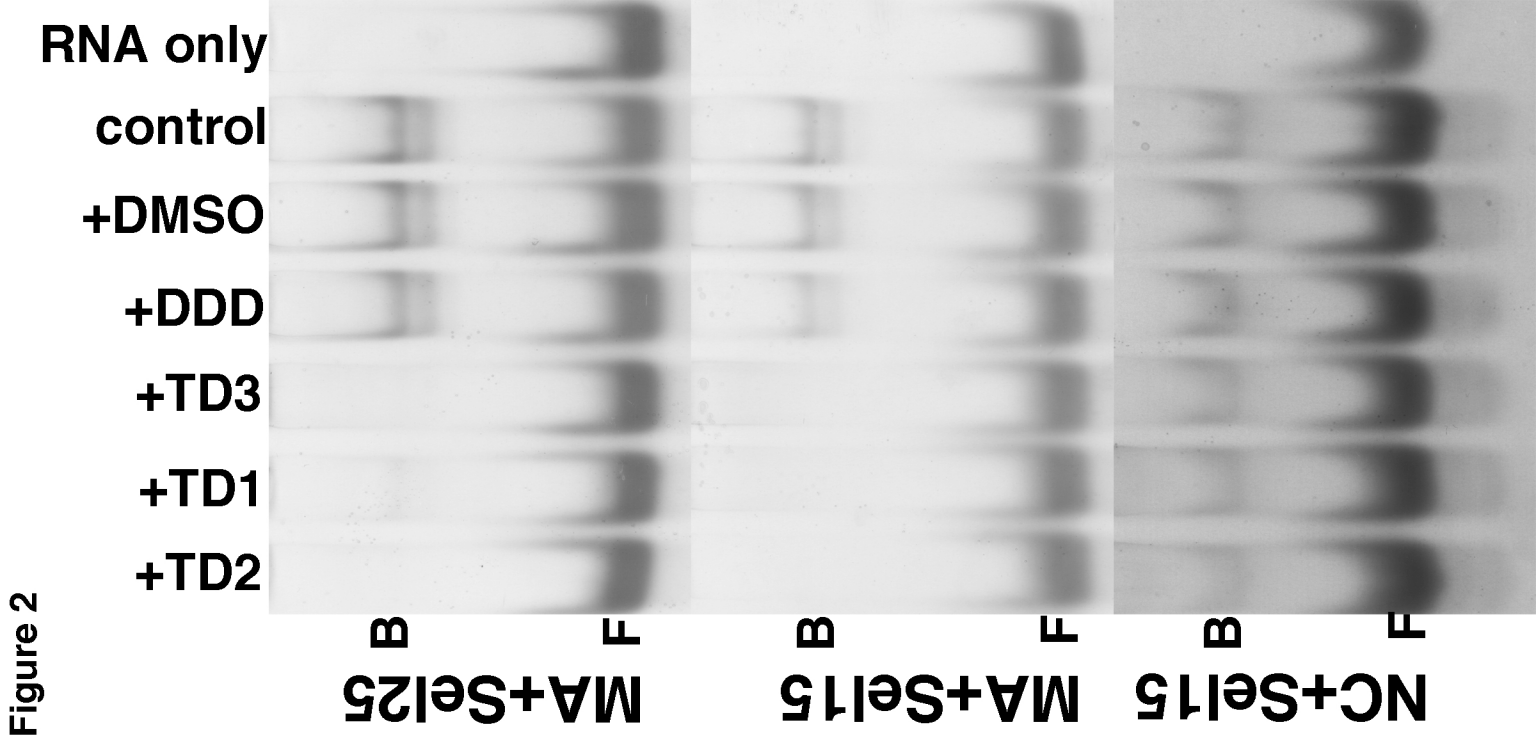
RNA only
control
+DMSO
+DDD
+TD3
+TD1
+TD2
B
F
MA+Sel25
B
F
MA+Sel15
B
F
NC+Sel15

Figure 2

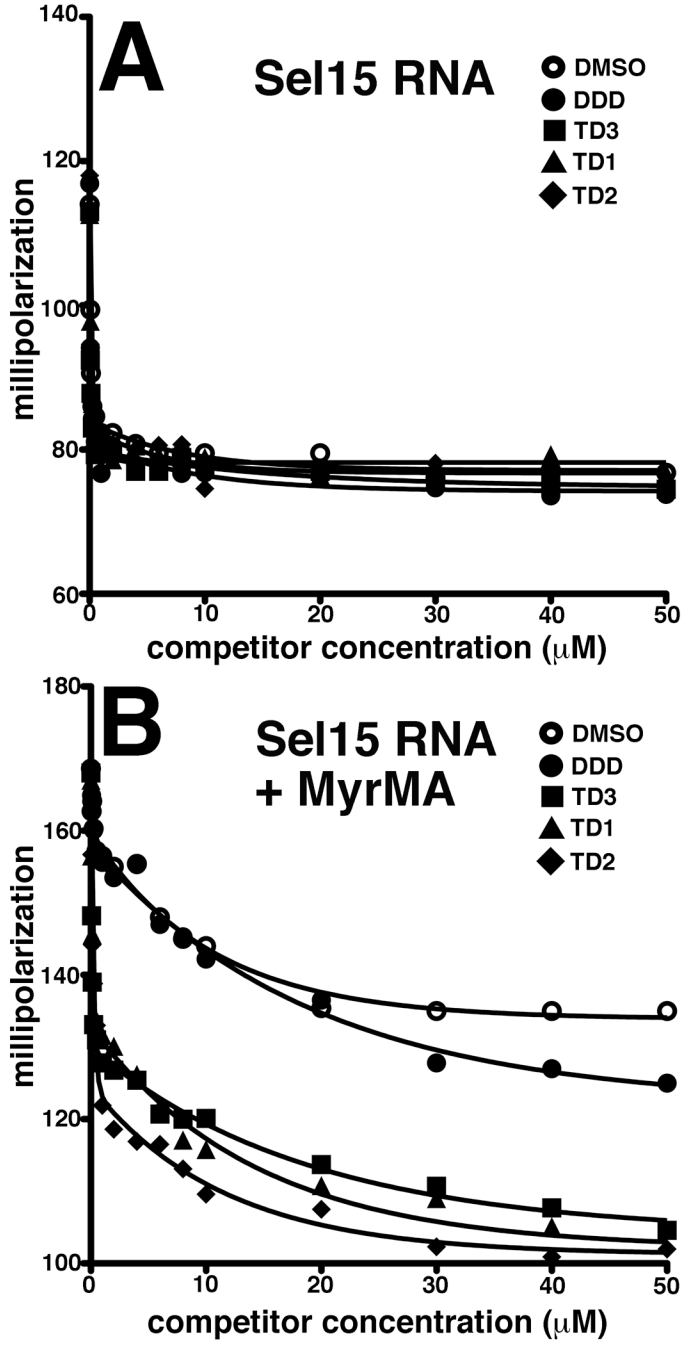
A
Sel15 RNA
DMSO
DDD
TD3
TD1
TD2
millipolarization
140
120
100
80
60
0
10
20
30
40
50
competitor concentration (μM)
B
Sel15 RNA
+ MyrMA
DMSO
DDD
TD3
TD1
TD2
millipolarization
180
160
140
120
100
0
10
20
30
40
50
competitor concentration (μM)

Figure 3

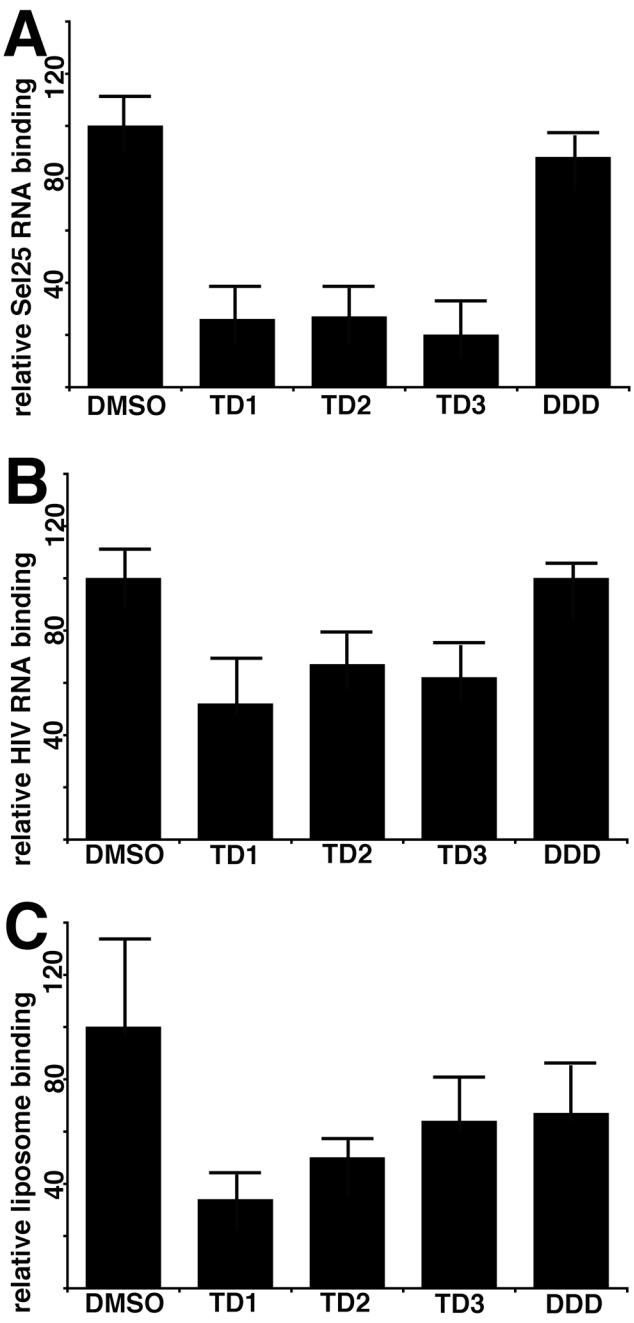
A
relative Sel25 RNA binding
120
80
40
DMSO
TD1
TD2
TD3
DDD
B
relative HIV RNA binding
120
80
40
DMSO
TD1
TD2
TD3
DDD
C
relative liposome binding
120
80
40
DMSO
TD1
TD2
TD3
DDD

Figure 4

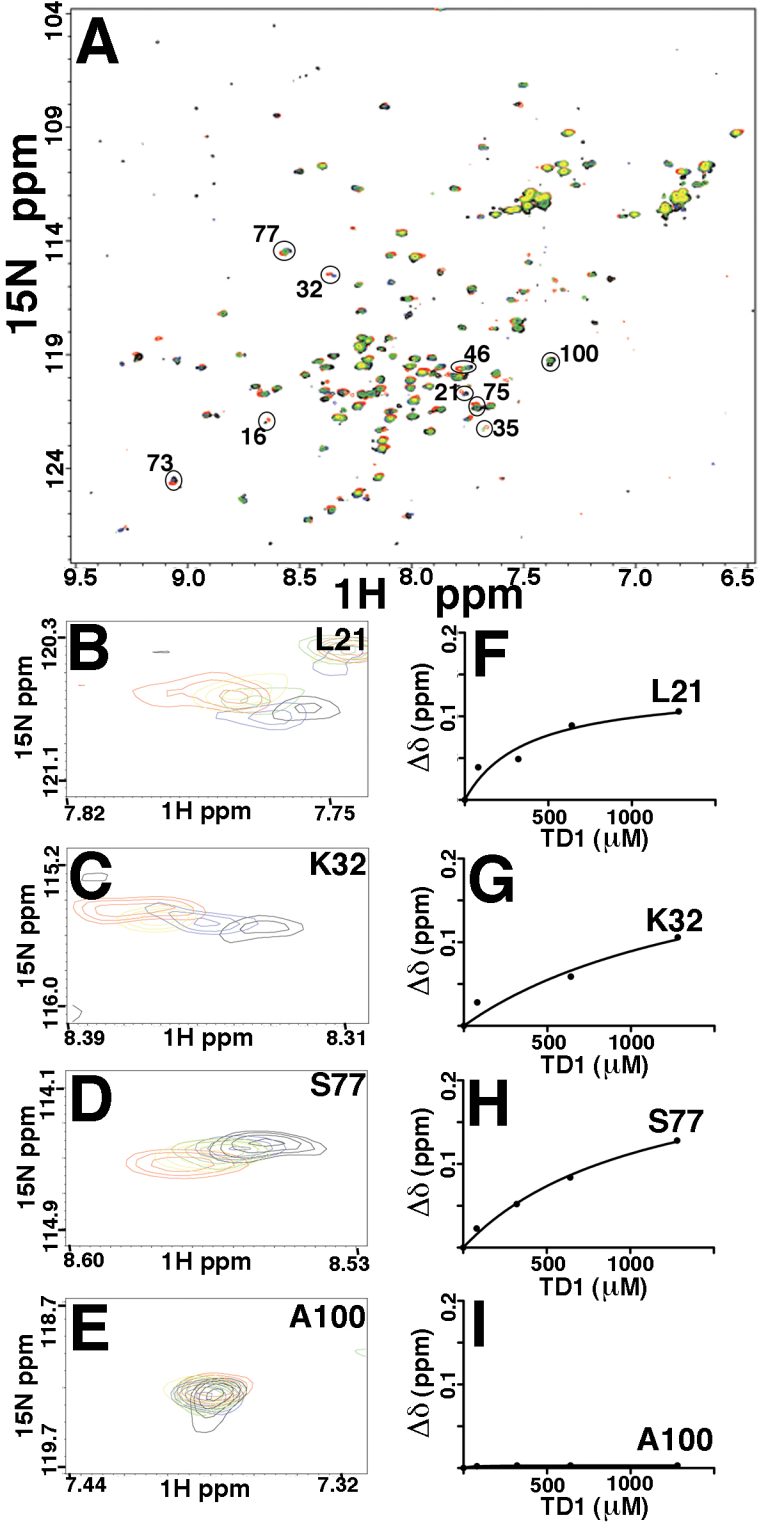

Figure 5

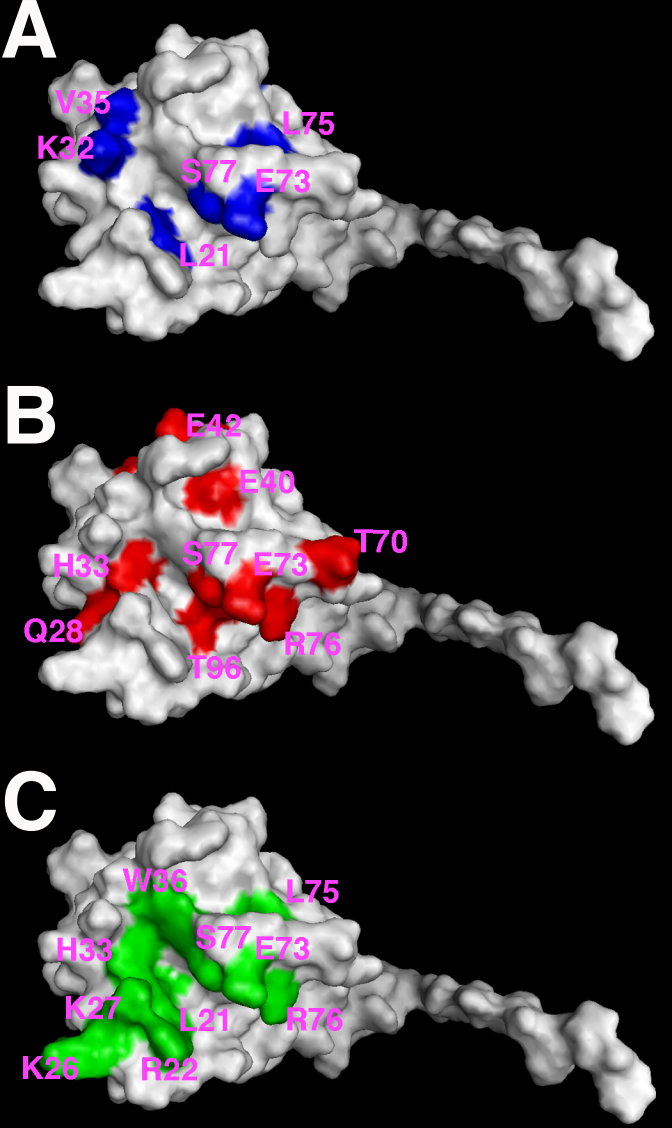

Figure 6

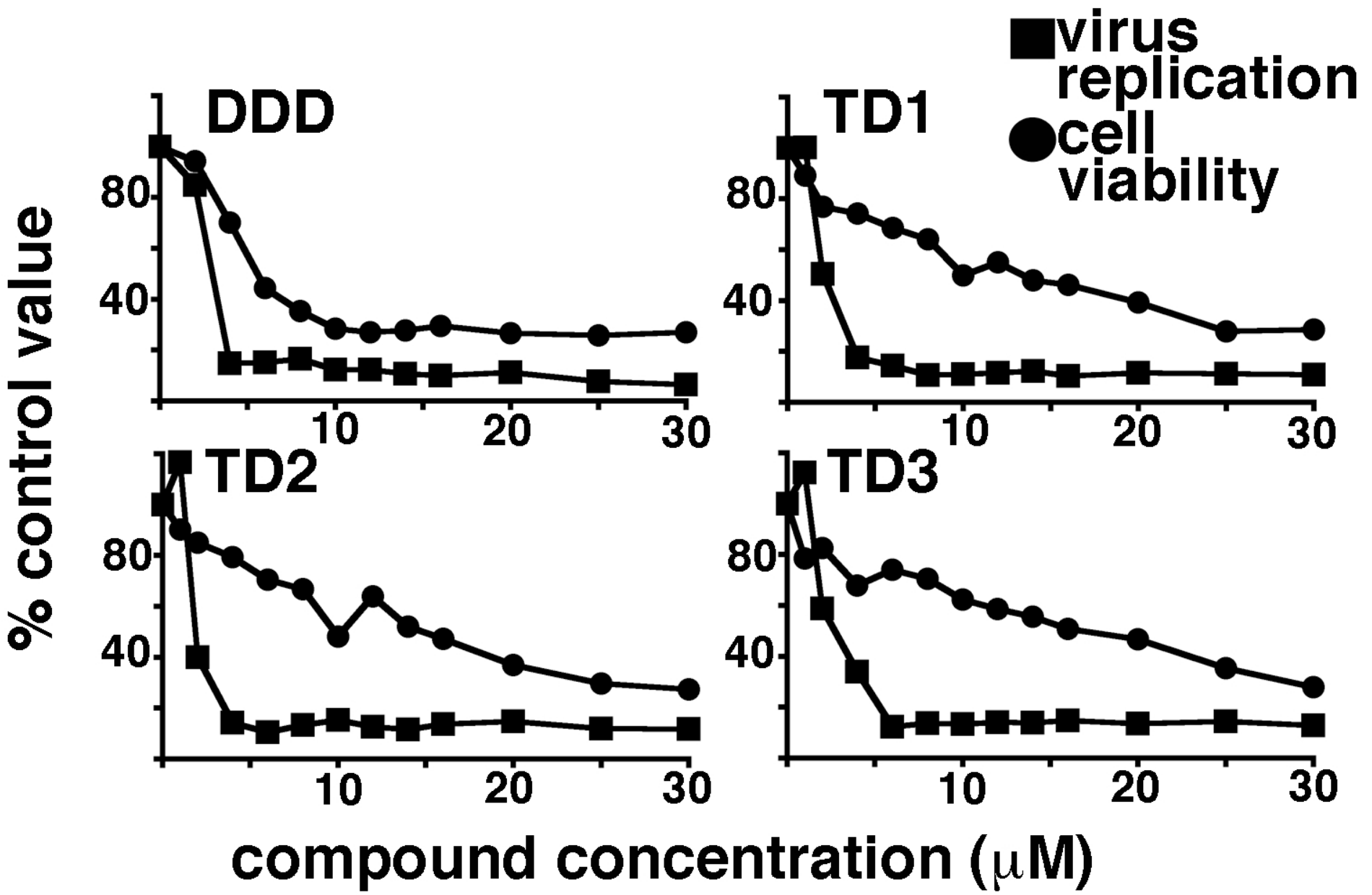
virus replication
cell viability
DDD
TD1
TD2
TD3
% control value
80
40
10
20
30
compound concentration (μM)

Figure 7

Supplementary Material Supplementary material can be found at:
http://www.jbc.org/content/suppl/2012/11/07/M112.399865.DC1.html